ELSEVIER

FEMS Microbiology Ecology 32 (2000) 181–196

FEMS MICROBIOLOGY Ecology

www.fems-microbiology.org

Phototrophs in high iron microbial mats: microstructure of mats in iron-depositing hot springs

Beverly K. Pierson *, Mary N. Parenteau

Biology Department, University of Puget Sound, 1500 N. Warner, Tacoma, WA 98416, USA

Received 13 November 1999; received in revised form 3 March 2000; accepted 3 March 2000

Abstract

Chocolate Pots Hot Springs in Yellowstone National Park are high in ferrous iron, silica and bicarbonate. The springs are contributing to the active development of an iron formation. The microstructure of photosynthetic microbial mats in these springs was studied with conventional optical microscopy, confocal laser scanning microscopy and transmission electron microscopy. The dominant mats at the highest temperatures (48–54°C) were composed of *Synechococcus* and *Chloroflexus* or *Pseudanabaena* and *Mastigocladus*. At lower temperatures (36–45°C), a narrow *Oscillatoria* dominated olive green cyanobacterial mats covering most of the iron deposit. Vertically oriented cyanobacterial filaments were abundant in the top 0.5 mm of the mats. Mineral deposits accumulated beneath this surface layer. The filamentous microstructure and gliding motility may contribute to binding the iron minerals. These activities and heavy mineral encrustation of cyanobacteria may contribute to the growth of the iron deposit. Chocolate Pots Hot Springs provide a model for studying the potential role of photosynthetic prokaryotes in the origin of Precambrian iron formations. © 2000 Federation of European Microbiological Societies. Published by Elsevier Science B.V. All rights reserved.

Keywords: Phototroph; Iron; Hot spring mat; Cyanobacterium; Microstructure

1. Introduction

Prokaryotes play major roles in the transformations of iron in the environment [1–4]. The most extensive studies of microbial iron oxidations have focused on the aerobic oxidation of iron in acidic environments by *Thiobacilli* and other bacteria [1]. The microaerophilic or aerobic oxidation of Fe(II) in circumneutral environments influenced by bacteria including *Gallionella*, *Leptothrix* and others has received renewed attention in recent years [2,5]. Bacterial reduction of Fe(III) to Fe(II) is common in anoxic environments and is a property of many organisms [3,4]. Straub et al. [6] described the anaerobic oxidation of Fe(II) by bacteria in circumneutral environments using nitrate as an electron acceptor. Ehrenreich, Widdel and others [7–9] isolated and described bacteria that are able to use photosynthesis to directly oxidize Fe(II) coupled to CO_2 fixation under anoxic conditions. The environmental cycling of iron is a complex process involving these biological influences as well as purely chemical or photochemical reactions [10].

Determining the relative contributions of various biotic and abiotic factors to the cycling of iron in modern environments is a daunting task. Attributing iron transformations to specific prokaryotic effectors in ancient environments is even more challenging. Nevertheless, iron and its putative direct or indirect microbial transformations have been implicated in major events in the Earth's history, including the origin of life [11,12], the origin and evolution of photosynthesis [12,13] and the origin of the banded iron formations (BIFs) in the Precambrian [14].

Photosynthesis is a common theme in two of the major theories offered to account for the putative role of early microbial metabolism in the oxidation of iron in the Precambrian. The presence of oxidized iron in BIFs is used as evidence for the earliest biological production of oxygen [14]. This early appearance of oxygen has been attributed to the evolution of oxygen-producing photosynthesis in ancestral cyanobacteria, marking an important event in the evolutionary history of photosynthetic metabolism [14,15]. The theory of the role of early cyanobacteria in

* Corresponding author. Tel.: +1 (253) 879-3353; Fax: +1 (253) 879-3352; E-mail: bpierson@ups.edu

0168-6496/00/$20.00 © 2000 Federation of European Microbiological Societies. Published by Elsevier Science B.V. All rights reserved.
PII: S0168-6496(00)00018-0

producing localized oxygen levels sufficiently high to result in BIFs was proposed and thoroughly developed by Cloud [14], who asserted that the oxidation of abundant Precambrian Fe(II) consumed the oxygen produced by ancestral cyanobacteria. Another theory suggests that anoxygenic phototrophs could have contributed to the accumulation of BIFs by directly oxidizing Fe(II) in the absence of molecular oxygen [16–21]. The recent discovery of iron-dependent photosynthesis [7–9,22,23] supports these latter interpretations.

We are investigating the possible role of both of these types of photosynthesis in contemporary high iron environments. Our goal is to clarify the potential contributions of these major evolutionary photosynthetic events to the environmental oxidation of iron during the Precambrian.

We have found major accumulations of cyanobacterial mats in thermal iron springs. Chocolate Pots Hot Springs in Yellowstone National Park have the most well-developed and diverse cyanobacterial mats that we have observed in a high iron environment. We have been studying the cyanobacterial mats at Chocolate Pots Hot Springs since we initially observed them in 1992. We selected this site not only because of the cyanobacterial mat development, but also because of the conspicuous iron deposits accumulating at these springs. This is an ideal environment in which to study the relationships of photosynthetic prokaryotes to the oxidation of iron and to the deposition of iron minerals. It is a potentially suitable site for finding records of biological involvement in contemporary as well as recent past mineralization processes that could be useful for assessing the putative role of microbial activity in the development of ancient iron formations. Others have recently begun analyses of the iron deposits at these springs [24–26].

In this paper, we report the structural characterization of the major photosynthetic iron mats in this thermal habitat and the physical association of the microorganisms with the iron sediments. We also describe the major phototrophs present. In Pierson et al. [27], we described the physiological ecology of the phototrophs in the mats. In that paper, we examined the potential environmental impact of the photosynthetic activity within the mats on the iron sediments and the effects of the presence of iron on the photosynthetic metabolism. To our knowledge, these two papers are the first description and analysis of the microbial ecology of major high density natural communities of phototrophic prokaryotes associated with a developing iron deposit. Parts of this work have been reported previously [28,29].

2. Materials and methods

2.1. Water analysis

Water was collected by siphoning into argon-filled bottles from the upper source (53.5°C) on the main mound of the springs on the east side of the river. One ml of concentrated sulfuric acid was added to one bottle for subsequent ammonia analysis. The bottles were stored on ice during transport. All analyses were done according to standard methods [30] within 48 h of collection. Additional samples were analyzed for iron several times at the site using the ferrozine assay [31,32]. Oxygen was measured with a YSI Model 51B oxygen meter (Yellow Springs, OH, USA). Sulfide was determined chemically [33] and with a microelectrode (#663 Diamond General, Ann Arbor, MI, USA) and reference electrode (#401 Diamond General) connected to an Oyster pH/mV and Temperature Meter (Extech Instruments Corp., Waltham, MA, USA). Calibrations were made with freshly prepared standard solutions of sodium sulfide. The pH was measured with narrow range papers (ColorpHast pH indicator strips, pH 4.0–7.0 and 6.5–10.0, EM Science, Gibbstown, NJ, USA) and with an electrode (#818 Diamond General) connected to a battery-powered field pH meter (Jenco portable pH meter, San Diego, CA, USA). Temperature was measured with a Fluke Model 52 K/J thermometer (Everett, WA, USA).

2.2. Conventional light microscopy

Bright field, phase contrast and epifluorescence micrographs of the microbial mats were obtained with a Nikon Microphot-FX. The dissection microscope micrographs were obtained with a Zeiss STEMI SV-8 outfitted with a Zeiss MC63 camera. Kodak Ektachrome Elite II 100 and 200 ASA films were used.

2.3. Confocal laser scanning microscopy (CLSM)

Samples of the microbial mats were prepared under a dissecting microscope (Zeiss STEMI SV-8). Pieces of freshly collected mat, or mat preserved with 8% formaldehyde, were vertically or horizontally sliced into longitudinal or transverse 1-mm-thick sections using a scalpel blade. A mat slice was then placed on its side on a clean slide and surrounded by four pillars of vaspar (1:1 mixture of paraffin and petroleum jelly) to a height slightly greater than the sample [34]. The mat was soaked in 20 μl of 0.025% acridine orange (Sigma, St. Louis, MO, USA) for 10 min to ensure stain penetration into the mat and rinsed twice with glass distilled water. A coverslip was placed on top of the pillars of vaspar and pressed down until it just reached the surface of the mat slice without deforming it. To stabilize the sample, 1.5% agarose was infilled from the side and the coverslip was sealed to the surface of the slide with melted vaspar. Because whole mat samples were used (1-mm-thick vertical sections were cut from the top 1–3 mm of mat) and viewed from the side, it was possible to accurately measure the depth of occurrence of various microbial and mineral layers from the

top down through the mat using the *x*,*y* dimensions on the microscope. Except for Fig. 5, all CLSM figures are views from the side oriented so that the top of the mat is at the top of the figure.

The epifluorescence of the samples was examined with a Zeiss LSM 210 confocal laser scanning microscope as described by Ghiorse et al. [34]. Acridine orange fluorescence of cells was viewed with a Zeiss 09 filter cube (450–490, FT510, LP520) and usually swamped chlorophyll (Chl) *a* autofluorescence. Confocal images were collected using a 25× oil immersion objective (NA 0.8), 8-s scan rate and 16-frame line averaging. A series of images was collected by Z-sectioning the sample to depths of 12.5–60 μm in 2.5- or 5-μm increments. Images were collected as TIFF files on the hard drive of the host computer and transferred to a 100MB Iomega Zip Disk (Roy, UT, USA). The files were opened directly into Adobe Photoshop 3.0.5 (Adobe Systems, San Jose, CA, USA) on a Macintosh PowerMac 6500/275. Brightness and contrast of the images were adjusted in some cases, otherwise no image processing occurred.

2.4. Transmission electron microscopy (TEM)

Samples were prepared by cutting 1-mm^3 pieces of mat with a scalpel blade under a dissecting microscope and embedding in 1% agar [35]. The agar blocks containing the cells were fixed on ice for 2 h in 2% glutaraldehyde, 1% acrolein and 0.2 M sodium cacodylate buffer, pH 6.5. Secondary fixation was performed on ice for 2 h in 1% osmium tetraoxide and 0.2 M sodium cacodylate. The blocks were embedded in Epon-112 (Tousimis, Rockville, MD, USA) and oriented so that sections were cut vertically through the mat, allowing viewing of different depths of the mat in a given section. The embedded cells were thin-sectioned (60–90 nm), stained with uranyl acetate and viewed with a Zeiss EM 109 at 50 kV.

2.5. Pigment analysis

Pigment analyses of the various mat communities were obtained as outlined by Pierson et al. [35,36]. For in vivo pigment spectra, cells were separated from the iron and broken by sonication in TSM buffer. Pigment extracts were prepared in absolute methanol saturated with magnesium carbonate. Spectra were obtained with a Shimadzu UV-1601 spectrophotometer (Columbia, MD, USA) and a Cary 2300 UV-Vis-NIR spectrophotometer (Varian-Techtron, Mulgrave, Australia).

2.6. Identification

Cyanobacteria and *Chloroflexus* were identified by morphology in combination with fluorescence microscopy and absorption spectroscopy.

2.7. Light penetration

Spectra of light penetration through the microbial mats were obtained with a LiCOR Li-1800 spectroradiometer (Lincoln, NE, USA) by using a fiber optic tip or layering mat on the remote cosine receptor as previously described [37]. All measurements were made in June and July on clear days at an elevation of 2100 m.

3. Results and discussion

3.1. Description of Chocolate Pots Hot Springs

The springs are located on both sides of the Gibbon River approximately 3 miles south of Norris Junction in Yellowstone National Park. On each bank, one major spring has built a large, conspicuous mound. We studied the sources on the east side of the river adjacent to the road. The largest mound is a fairly steep sinter deposit that is 2–20 m wide and approximately 15 m long that extends down into the river (Fig. 1A). Several smaller sources or seeps occur along the steep banks and in the grassy meadow next to the river (Fig. 1B). Most of the sinter is covered with very shallow (0.1 to a few cm deep) rapidly flowing water. Flow rates vary considerably over small distances but rates of 20–50 cm s^{-1} are common.

3.2. Chemistry

The temperatures of the emergent source waters ranged from 51 to 54°C and cooled to as low as 37°C. The pH of the emergent water ranged from 5.8 to 6.0 and increased

Table 1
Water analysis of Chocolate Pots Hot Springs

Substance	This study (mg l^{-1})	Allen and Day [38] (mg l^{-1})
Aluminum	0.17	0
Ammonium nitrogen	< 1	ND[a]
Bicarbonate	248	353
Calcium	20	25
Carbonate	0	0
Chloride	28	29
Iron(II)	5.1	6.3
Iron(III)	< 0.1	0
Magnesium	3	1.0
Manganese	1.04	1.9
Nitrate nitrogen	< 0.2	ND
Nitrite nitrogen	< 0.2	ND
Potassium	24	31
Phosphorous	0.01	ND
Silica	159	98
Sodium	102	114
Sulfate	32	28
Sulfide	0	0

[a]Not determined.

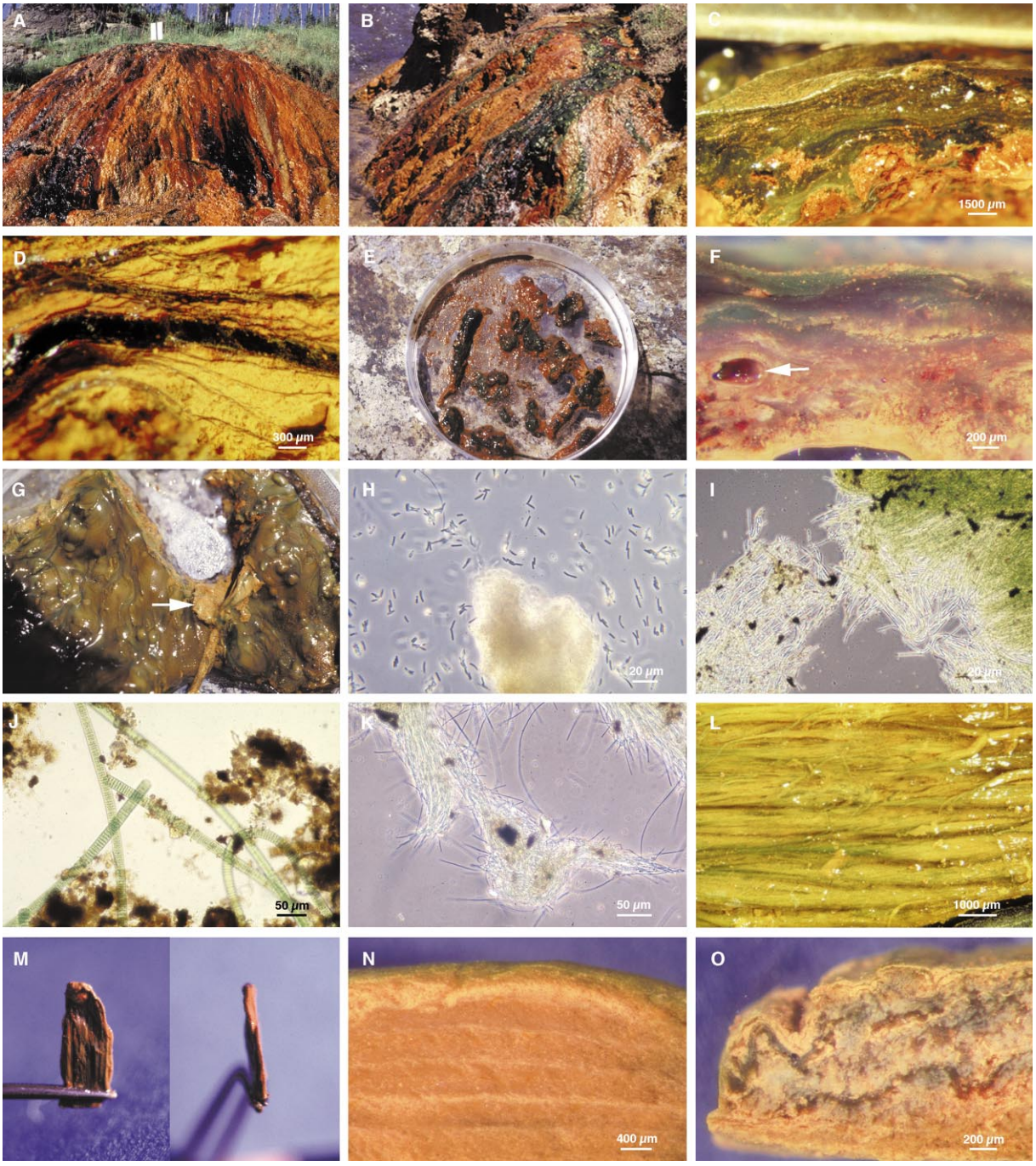

to as high as 7.0. The predominant ions in the source water were bicarbonate, silica and sodium (Table 1). No sulfide was detected in the source water. The analysis in Table 1 shows the high level of ferrous iron (5.1 mg l^{-1}) and low ferric iron (less than 0.1 mg l^{-1}) obtained with the phenanthroline method [30] on the nearly anoxic source water. Higher values for the concentration of ferrous iron in the source water (up to 9.5 mg l^{-1}) were obtained with the ferrozine assay [31,32], and all iron values other than those reported in Table 1 were obtained with this method. As the water flowed rapidly down the main mound, the ferrous iron levels decreased to about 2–4 mg l^{-1} and the oxygen increased from less than 1.0 mg l^{-1} to about 6 mg l^{-1} [27].

The chemistry of the Chocolate Pots Hot Springs source waters and the sinter formations are unique in Yellowstone National Park. The data from our water analysis (Table 1) and that published by Allen and Day in 1935 (Table 1) [38] are similar enough to substantiate the constancy of the environment since the 1930s. The initial description and naming of the unique mounds, 'Chocolate Pots' in the late 19th century, further document the con-

Fig. 1. (A) Main mound iron formation being deposited at Chocolate Pots Hot Springs. The main source is at the top of the mound where the white sign is posted. Warm water cascades over the face of the mound in thin sheets. The colors are due to the mineral deposits and some mats. (B) Source (51–52°C) of rapidly flowing water with thick *Pseudanabaena*/*Mastigocladus* mat developed on the iron formation near the base of the main mound. (C) Vertical section through mat shown in (B) showing layers of cyanobacteria flecked with iron oxides throughout and layered with iron oxides most conspicuously near the base of the mat. (D) Layered iron deposit with alternating glassy (dark) and iron oxide (orange) layers removed from main mound adjacent to mat. (E) Pieces of hardened iron oxides coated with *Synechococcus* mat removed from near the main source (52°C) and placed in a standard Petri dish. (F) Vertical section through *Synechococcus*-impregnated iron deposit collected at 52°C showing dense *Synechococcus* surface layers (green), accumulating iron oxides (red/orange) and red glassy deposit (arrow) amid gelatinous iron oxide accumulations. (G) Top view of olive mat in a Petri dish showing trapped oxygen bubbles. The surface layer of the mat has been peeled back (arrow) to reveal the cohesive iron deposit underneath. (H) Phase contrast micrograph of *Synechococcus* mat with rod-shaped cells and a large granule of iron oxides. (I) Phase contrast micrograph of *Pseudanabaena* mat with iron oxide granules. (J) Bright-field micrograph of *Oscillatoria* cf. *princeps* and iron oxide deposits. (K) Phase contrast micrograph of narrow *Oscillatoria* filaments with iron oxide granules. (L) Streamers of narrow *Oscillatoria* filaments and iron oxides oriented parallel to direction of water flow on surface of rigid mat. (M) Heavily mineralized rigid olive mat, 2-mm-thick, that retains its shape when held in the air with forceps. Actual size. (N) Vertical section of a thick, highly layered olive mat photographed through a dissecting microscope. Top dense green layer of thin *Oscillatoria* measures approximately 0.2 mm. Thicker, more transparent gel-like layers alternate with dense iron oxide layers. This mat was very cohesive and contained scattered filaments in the upper gel layers visible with higher magnification. (O) Vertical transverse section of rigid mat shown in (M) photographed through a dissecting microscope. Cauliflower-shaped deposits of clear gel-like layers alternate with iron oxides and are covered with thin filaments. Section was cut perpendicular to the direction of water flow.
←

stancy of this high iron thermal environment for at least 100 years [39].

The iron(II) levels we measured of 5.1–9.5 mg l^{-1} are equivalent to about 100–170 μM Fe(II), which is less than the 250-μM Fe(II) levels detected in the iron cold spring studied by Emerson and Revsbech [31]. However, the concentration of iron in Chocolate Pots water is 100–1000 times higher than the levels of Fe(II) found in most neutral thermal springs in the park [38,40,41]. The well-studied Octopus Spring contains iron levels of 1.4–2.8 μg l^{-1} at the source [41].

The presence of high levels of ferrous iron in the emerging waters accompanied by high concentrations of silica and bicarbonate create a sinter deposit of distinctive color and composition (Fig. 1A). Variations in the mineralogy produce a deep orange iron oxide streaked with brighter yellow, deeper reds, browns and black. Allen and Day [38] analyzed this sinter and found it unlike anything else in the Yellowstone thermal areas. It is a fine-grained amorphous mixture of iron oxides and silica that is highly hydrated and contains about 55% ferric oxide, 17% silica, 19% water and small amounts of aluminum and manganese oxides.

The lack of crystalline structure in the mineral deposits at Chocolate Pots makes specific identification of the amorphous iron compounds on a fine scale difficult. Agresti et al. [24] and Wade et al. [25] used Mössbauer and XRD analysis on samples collected at different distances from the sources and at different depths in the sediments. They reported the presence of amorphous ferrihydrite dominating the surface sediments and the vent sources and detected nontronite, hematite and goethite in most samples. They reported the presence of laminated glasses of alternating bands of clear (possibly quartz) and ferric deposits that could be similar to laminated deposits we observed (Fig. 1D). Siderite ($FeCO_3$) was found only below the top mm of sediments and mostly downstream from the vents [25].

3.3. Gross description of phototrophic mats

We have observed four major and fundamentally different types of mats. At the highest temperatures (49–54°C), a very thin mat (0.5–1.0 mm) composed of*Synechococcus* sp. and *Chloroflexus* sp. was distributed in patches directly on top of hardened mineral deposits (Fig. 1E,F). The thin cyanobacterial surface layer impregnated with unconsolidated iron grains was directly above layers of orange and red compacted mineral deposit (Fig. 1F). In rapidly flowing water at some high temperature sources, floating streamers and thick (2 to several mm) gelatinous mats composed primarily of layers of *Pseudanabaena* impregnated with iron granules developed above consolidated orange iron deposits (Fig. 1B,C). At lower temperatures (37–47°C) in quieter pools, *Oscillatoria* cf. *princeps* formed floating or surface dwelling mats which were usually associated with a metallic, surface scum that fractured when disturbed.

The majority of the cohesive microbial mats from 36 to 45°C were composed primarily of a highly motile, narrow filamentous cyanobacterium that resembles an *Oscillatoria*. The color of the 1–2-mm-thick mats was usually an olive green, due to the presence of considerable orange mineral deposit associated with the green filaments (Fig. 1G). Oxygen bubbles accumulated within these mats during the day (Fig. 1G).

Thick, gelatinous olive mats had a very thin (0.2–0.5 mm), dense layer of green *Oscillatoria* filaments on the surface. This film capped a laminated orange mineral layer sometimes several mm-thick (Fig. 1N). The laminations of dense orange mineral accumulations alternated with less dense clear gelatinous layers (Fig. 1N). Scattered *Oscillatoria* filaments were also observed deeper in the mat within the gelatinous layers.

Some of the olive mats were so thoroughly impregnated with minerals that even very thin pieces were rigid and retained their shape when removed from the water (Fig.

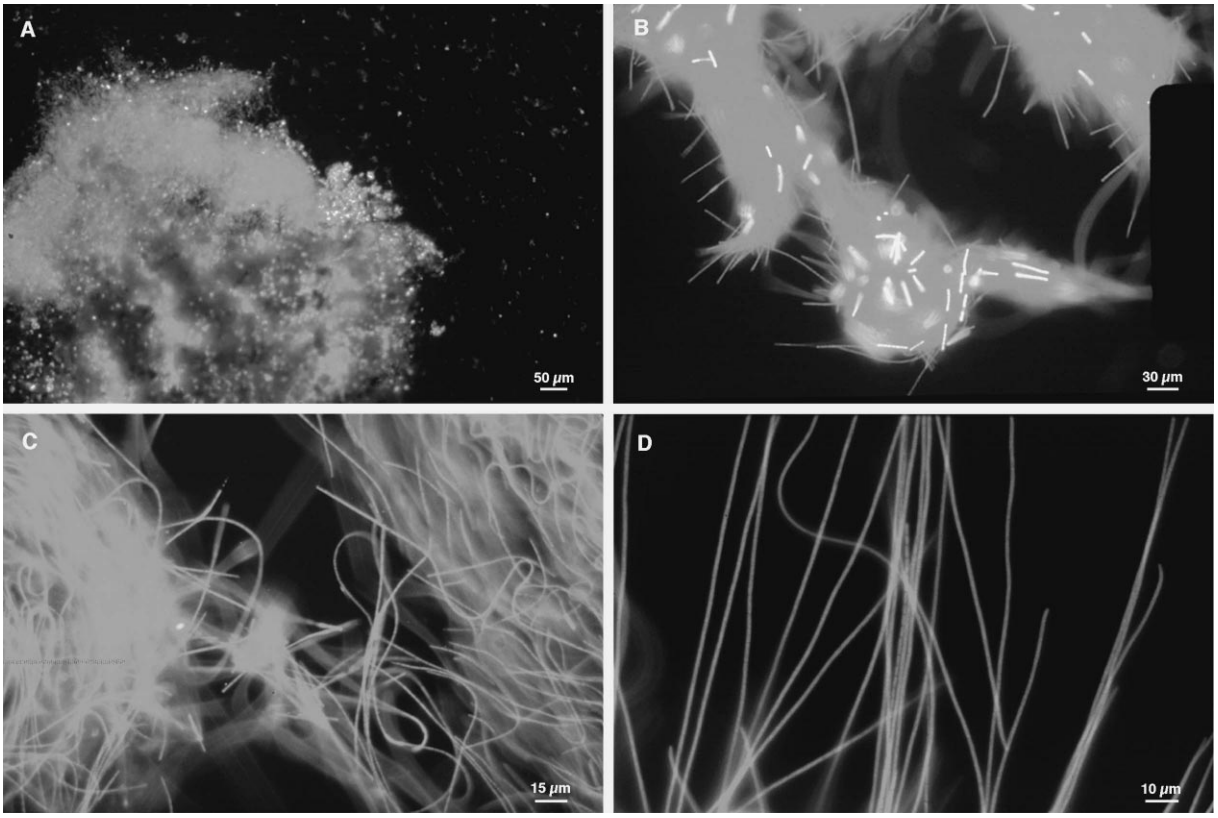

Fig. 2. Photomicrographs showing red Chl *a* and phycocyanin autofluorescence as gray and yellow phycoerythrin autofluorescence as brighter white. (A) Iron oxide granule illuminated from within by the high density of red fluorescent *Synechococcus* cells with some brighter spots from *Cyanothece*. (B) Olive mat shown in Fig. 1K with narrow red fluorescing *Oscillatoria* filaments (gray) and short filaments of yellow fluorescing *Pseudanabaena* (brighter). (C) Nearly pure masses of narrow *Oscillatoria* filaments in an olive mat. (D) Filaments of narrow *Oscillatoria* gliding out in parallel array from a piece of olive mat.

1M). Although less obviously laminated, they had a dense olive green surface layer on top of a cauliflower-like region of orange mineral layers alternating with clear gelatinous layers (Fig. 1O). Sometimes the olive mat filaments were organized in streamers (Fig. 1L).

Most of these mats had a fine-structured layering of the concentrated iron oxides with clearer gel-like layers (silica?) sometimes containing scattered cyanobacterial filaments. All were capped by a dense surface layer of cyanobacteria (Fig. 1F,N,O). These layered, active cyanobacterial mineral mats bear structural resemblance to the hard, finely laminated iron and silica mineral deposits of the mound (Fig. 1D). Since we have not yet analyzed the mineralogy of the iron mats, we cannot say how similar they are to the sinter deposit or to finely layered BIFs.

3.4. Optical microscopy

Typical *Synechococcus* cells (1.5 μm in diameter and 4.5–9.0 μm long) and an occasional filament (less than 1 μm in diameter and possibly *Chloroflexus*) were observed along with abundant orange/red mineral granules in the green surface layer of the high temperature mats (Fig. 1H). Deeper in the mat, cells were difficult to detect using conventional microscopy because they were intimately associated with the amorphous mineral deposits. However, the intense red autofluorescence of the Chl *a*-containing *Synechococcus* cells (Fig. 2A) illuminated the mineral granules in which the cells were densely embedded. Unicellular ovoid to coccoid cyanobacteria rich in phycoerythrin, *Cyanothece minnervae* (3–4 μm in diameter), fluoresced yellow. The putative *Chloroflexus* filaments did not visibly fluoresce. As noted by Emerson and Revsbech [31] and Emerson and Moyer [5], we found that fluorescence microscopy was essential for detecting cells among amorphous iron precipitates of similar dimensions.

Two different sizes of the *Pseudanabaena* filaments were noted at 2.5-μm and 3–4-μm diameter. The individual filaments were often embedded in and surrounded by mineral deposits (Fig. 1I). Branching *Mastigocladus* filaments were sometimes present.

Oscillatoria cf. *princeps* filaments (17–18 μm in diameter) were intimately associated with orange iron oxide deposits (Fig. 1J). They had slightly hooked ends and prominent terminal cell wall burs (Fig. 1J).

The filaments of the narrow *Oscillatoria* comprising the wide-spread olive mats were 1.5 μm in diameter, indeterminate in length and had hooked ends (Fig. 2D). In addition to the thin *Oscillatoria* filaments, olive mats frequently contained *Synechococcus*. *Pseudanabaena* and *C.*

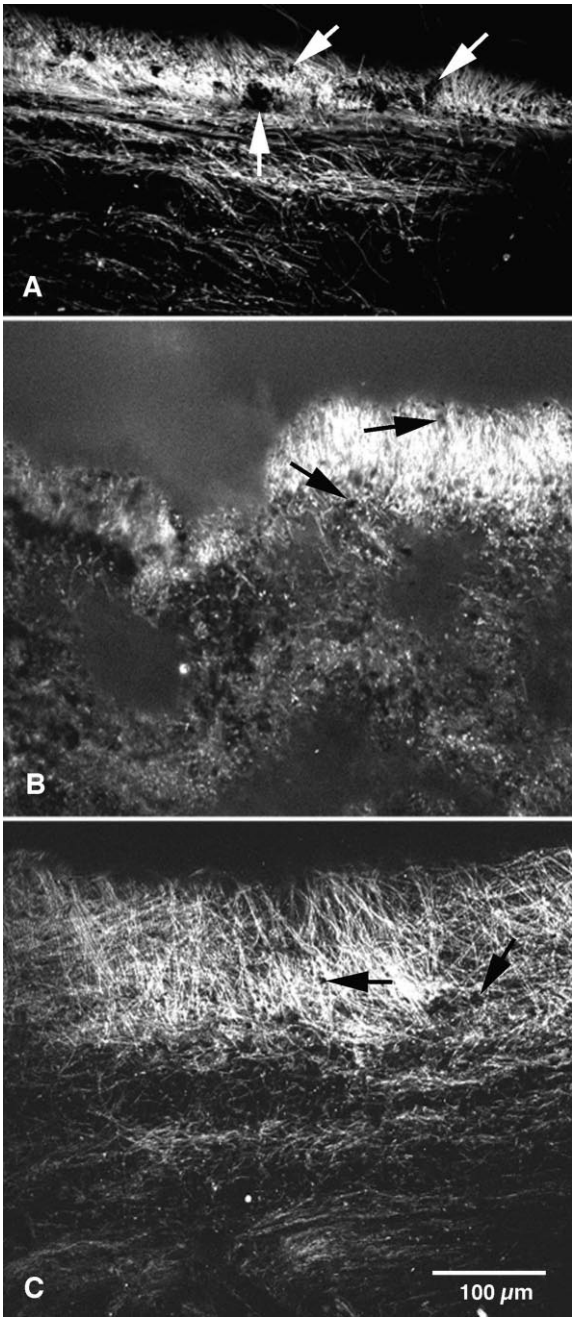

Fig. 3. Confocal laser scanning micrographs of vertical sections through acridine orange-stained olive mat. The scale bar marker in (C) applies to all three figures. (A) Section cut at slightly oblique angle shows fairly large iron oxide granules (white arrows) embedded among vertically oriented surface filaments of narrow *Oscillatoria*. Beneath this layer, filaments are oriented horizontally among iron deposits. (B) Vertically oriented dense lawn of narrow *Oscillatoria* filaments with numerous entrapped iron granules (black arrows). Voids in the mat below the surface were filled with rigid gel-like material (depositing silica?). Iron oxide granules can be seen throughout. Bright spots below the surface are cut ends of horizontally arrayed filaments oriented perpendicular to the plane of the section. (C) Vertical section through a thick olive mat of dense vertically oriented surface filaments with entrapped iron grains (black arrows) and less dense layers of horizontally and randomly oriented filaments alternating with layers of iron beneath the surface.

minnervae were detected in some of these mats by their yellow phycoerythrin autofluorescence (brighter fluorescence in Fig. 2B). Other mats were nearly pure *Oscillatoria* (Fig. 2C). Above 45°C, *Synechococcus* increased in abundance, and below 40°C, many other cyanobacteria were mixed in with the still abundant filaments. Some of the narrow *Oscillatoria* filaments were intimately associated with mineral deposits (Fig. 1K).

Some of the iron sediments had no mats on the surface (not shown). Low densities of cyanobacteria were occasionally detected by Chl *a* autofluorescence among the sediment particles. Staining of sediments with DAPI and acridine orange revealed the presence of very thin filaments (less than 1.0 μm) and unicells that did not autofluoresce, indicating the absence of photosynthetic pigments. We did not detect the distinct morphological forms of *Leptothrix* or *Gallionella* in any of these sediments or mats and have not identified the chemotrophs present.

3.5. CLSM

With CLSM, we could observe the internal relationships in fully hydrated dense mats without disturbing the native mat microstructure. The mats were viewed as fresh, live specimens unaltered accept for the application of acridine orange or were preserved with formaldehyde immediately upon removal from the hot spring. We were able to optically penetrate to depths of 75 μm in thick sections of native mat using a long working distance 25× objective. Laser sectioning in 2–5-μm increments over depths of 60–70 μm allowed us to reconstruct three-dimensional images (data not shown), permitting visualization of mineral/bacterial structural relationships. We had little difficulty getting rapid and reproducible results with our procedure using mm-thick pieces of dense microbial mat. Background fluorescence from acridine orange in our preparations was minimal or non-existent. Little et al. [42] also found CLSM useful for observing bacteria intimately associated with iron minerals.

The CLSM images of acridine orange-stained whole mats revealed structural details of the unaltered native mat that were impossible to observe with conventional microscopy. The narrow *Oscillatoria* filaments in the surface layers of several samples of olive mat were densely packed and often vertically oriented, forming a lawn of filaments (Fig. 3A–C). A similar vertical lawn of filaments was also observed in the *Pseudanabaena* mat (Fig. 4). Mineral granules could be seen trapped within these layers among the filaments in both olive and *Pseudanabaena* mat (arrows in Figs. 3A–C and 4).

Beneath the surface layer of narrow *Oscillatoria* filaments in olive mat, an irregular layer of mineral deposit covered deeper layers of horizontally or randomly oriented filaments (Fig. 3A–C). When the dense surface layer of filaments was removed and the microscope was focused

Fig. 4. Cortical laser scanning micrograph of vertical section cut through the top mm of *Pseudanabaena* mat perpendicular to direction of water flow and stained with acridine orange. White arrows indicate dark iron oxide deposits. Filaments in the top 150 μm are vertically oriented. Beneath the surface, the filaments form conspicuous layers with a horizontal orientation, often in highly parallel arrays. The filaments appear to have a purely random orientation only at the bottom of the section.

down vertically into the lower layers of mat, randomly oriented filaments were revealed, some of which were encased in mineral deposits (Fig. 5). Under the vertical lawn of filaments in the *Pseudanabaena* mat, arrays of roughly parallel filaments also occurred in horizontal layers (Fig. 4). These stacked parallel arrays of filaments formed a sheet-like layering pattern seen in the 3–5-mm-thick whole mat (Fig. 1C).

CLSM more clearly revealed the prominence of thin *Chloroflexus* filaments (approximately 0.8-μm diameter) in the *Synechococcus* mat than conventional optical microscopy. In the top 200–300 μm of some mats, the *Synechococcus* cells were so abundant that their fluorescence obscured the filaments (Fig. 6A). However, in other regions of the surface (Fig. 6B) and where the surface of the mat was slightly torn (Fig. 6A),*Chloroflexus* filaments could be detected (white arrow in Fig. 6A). In the deeper parts of the mat (300–500 μm), *Synechococcus* and *Cyanothece* cells were relatively less abundant (Fig. 6C,D). The *Chloroflexus* filaments were more conspicuous at these depths and they alone appeared to be the major anchoring force of the mat to the hard sediments below 500 μm (Fig. 6D). Mineral granules were also conspicuous in the *Synechococcus*/*Chloroflexus* mat (arrows in Fig. 6A–D). This vertical distribution of *Synechococcus* and *Chloroflexus* is similar to that observed in mats in neutral or alkaline hot springs low in iron, such as Octopus Spring in Yellowstone and Hunter's Hot Springs in Oregon, where the abundance of *Synechococcus* relative to *Chloroflexus* also decreases with depth [43]. As in Chocolate Pots, *Chloroflexus* is clearly present throughout these thicker mats, even at the surface [43].

The occurrence of *Chloroflexus* in the mats at Chocolate Pots is contrary to reports that it is not found in high iron thermal springs [44]. Given the difficulty of detecting *Chloroflexus* microscopically among the iron sediments except when acridine orange staining is used, it is possible that it was overlooked in samples from iron springs during the extensive survey of its distribution in hot springs in Japan [44]. The enrichment medium used [44] may have failed to sustain *Chloroflexus* from high iron environments. As in other well-studied *Synechococcus*/*Chloroflexus* mats found in non-sulfidic hot springs, it is assumed that the photoautotrophic activity of the *Synechococcus* provides the organic carbon source for the photoheterotrophic *Chloroflexus* [45]. It is tempting to suggest by analogy to sulfide springs in which *Chloroflexus* grows at higher temperatures than cyanobacteria as a sulfide-dependent autotroph [45], that the high level of Fe(II) in the source water could be sustaining an iron-dependent photoauto-

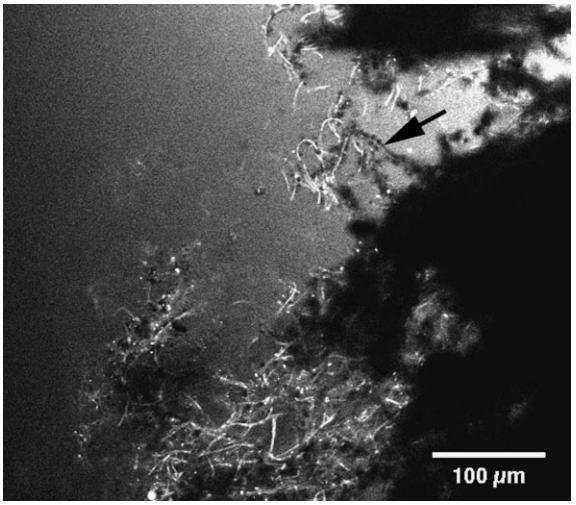

Fig. 5. Cortical laser scanning micrograph of horizontal section through acridine orange-stained olive mat. The densely packed layer of surface filaments was removed by slicing off the top 200–500 μm of mat. The microscope was focused down vertically into the lower mat through a gap in the layer of iron deposit (dense black layer on right of figure) that accumulated beneath the surface layer of filaments. Filaments were much less densely packed than in the surface layer and were randomly oriented at this depth. Occasional iron-encased filaments were seen (black arrow).

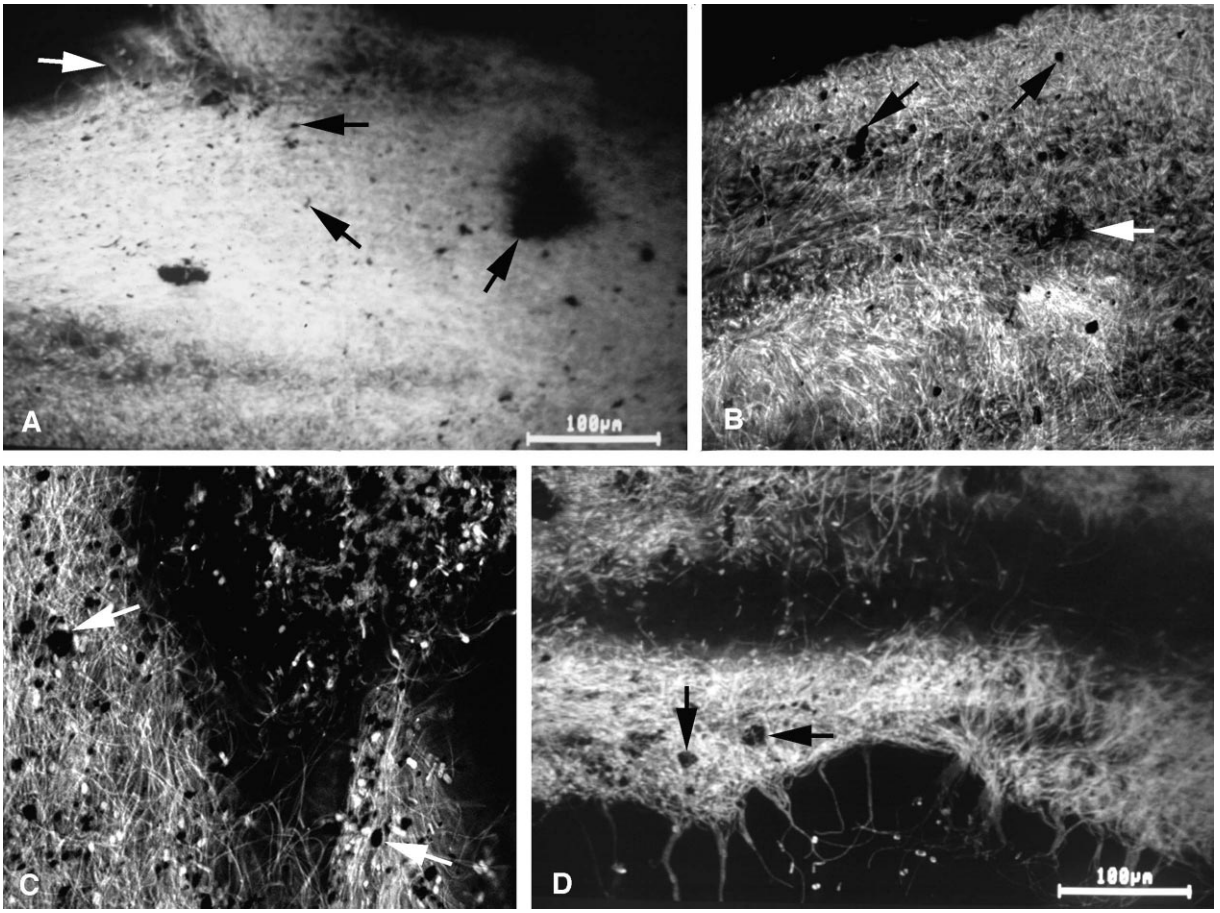

Fig. 6. Confocal laser scanning micrographs of *Synechococcus* mat. Vertical sections of mat were cut to a thickness of 1 mm, stained with acridine orange and viewed with a confocal laser scanning microscope (Zeiss LSM 210) using epifluorescence. The 100-μm bar markers apply to all four figures. (A) The fluorescence is so bright in the top 300 μm due to the densely packed *Synechococcus* cells that it is difficult to discern other features except for the dense iron oxide granules (black arrows). At the very surface where the mat is slightly torn, filaments of *Chloroflexus* can be seen (white arrow). (B) Other regions near the surface that are less densely packed reveal the filamentous meshwork of *Chloroflexus* among the *Synechococcus*. Iron granules are seen throughout (arrows). (C) Deeper in the mat, the density of *Synechococcus* decreases and the *Chloroflexus* filaments are more prominent. Iron oxide granules occur throughout (arrows). (D) At the base of the mat (around 500 μm from the surface in this case), the *Chloroflexus* filaments are more conspicuous than the *Synechococcus* cells and extend like tethers into the iron substrates below. Arrows indicate iron granules.

trophy in *Chloroflexus* upstream from the cyanobacteria [27]. The high concentrations of reduced iron at the highest temperatures near the sources may be inhibiting the cyanobacteria from forming mats as does sulfide in other springs.

3.6. Role of motility in trapping and binding of iron sediments

The vertical orientation of filaments in the CLSM indicated possible light-dependent motility contributing to a lawn which could bind and trap sediment particles. Gliding of *Oscillatoria* was observed microscopically (Fig. 2D) and in response to light. When mats were covered in situ with a fine mesh screen, filaments aggregated under the holes in the screen. When small clumps of amorphous oxidized iron particles less than 1.0 mm in diameter were sprinkled on the surface of olive cyanobacterial mat in situ, they became stuck to the mat within 2 h. Microscopic examination of such clumps showed them to be totally covered and impregnated by masses of the narrow *Oscillatoria* filaments.

The development of sediment-stabilizing mats at Chocolate Pots is a light-dependent process. To test this hypothesis, we stripped off a small area of 1.0-mm-thick olive mat of *Oscillatoria* filaments covering unconsolidated sediments at 39°C on the main mound. Two adjacent areas of the remaining loose sediment were monitored for 10 days, one exposed to ambient light and one covered to remain dark. After 10 days, the area exposed to the light had developed a cohesive mat that covered and stabilized the sediments. This mat was microscopically identical to the original one that had been removed. In the dark, no mat developed and the sediments remained loose and flocculant. No viable cyanobacteria and no conspicuous populations of chemotrophs were observed.

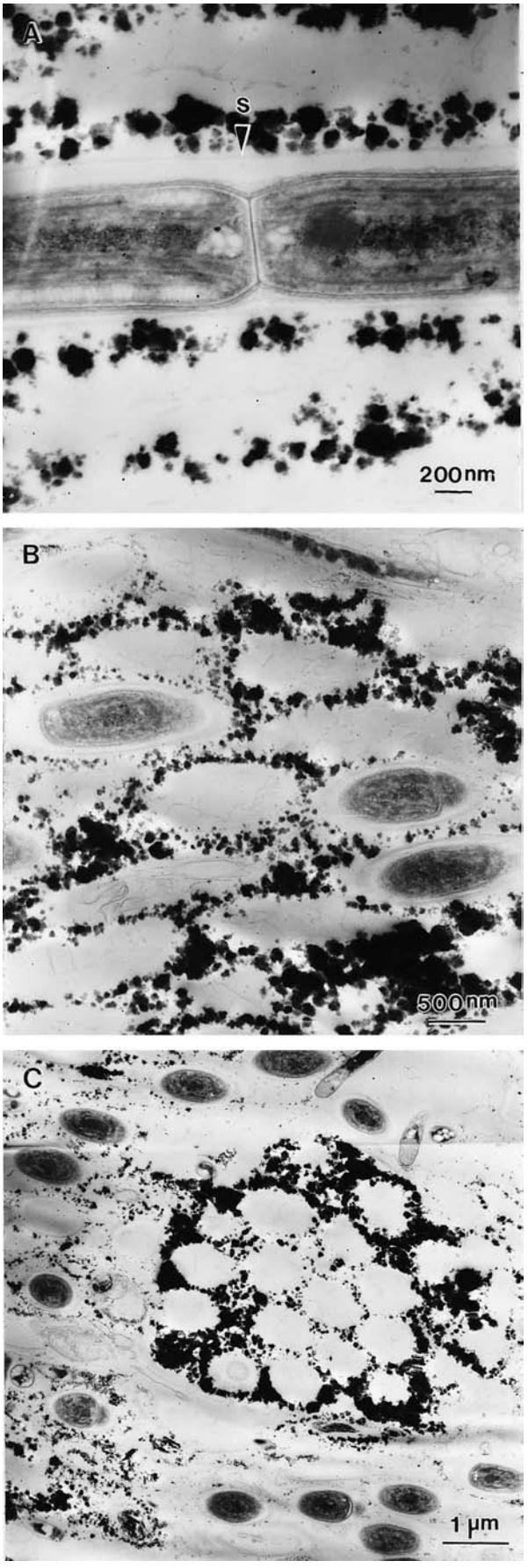

3.7. TEM

Electron microscopy of fixed and thin sectioned olive mat revealed parallel arrays of membranes around the periphery of the cytoplasm and a thick sheath exterior to the *Oscillatoria* filaments (Fig. 7A). Substantial mineral deposits surrounded individual filaments and appeared to accumulate in the extracellular matrix external to the actual sheath material (Fig. 7A,B). Well-preserved cells could be seen in sections of some mineral casts, while others appeared empty (Fig. 7B). Frequently, filaments were encased in parallel arrays, forming a cylindrical packet of filaments (Fig. 7B,C) resembling a streamer (Fig. 1L).

Electron microscopy of thin sections of *Synechococcus* mat revealed a microbial community embedded in a matrix within which minerals were deposited. In the deeper portions of the mat, cells were heavily encased with mineral deposit (Fig. 8A). Most of the heavily encased cells were degrading but sufficient cellular detail was preserved to identify concentric layers of membrane typical of *Synechococcus* and other unicellular cyanobacteria (Fig. 8A). At the surface of the mat, there was much less mineral deposit and the cells were better preserved. The diverse phototrophs included *Cyanothece*, *Synechococcus* and *Chloroflexus*, as well as unidentified small rods (less than 0.5 μm in diameter) that contained concentric rings of peripheral membranes (Fig. 8B).

The cyanobacterial mats at Chocolate Pots appear to have at least a passive role in contributing to iron deposition and mound growth. Extracellular polysaccharides and cell wall materials have been described as passive accumulators of iron oxides, silica and other minerals in bacteria, including cyanobacteria [46–49]. The copious extracellular sheaths and matrices (probably polysaccharides) seen in the transmission electron micrographs of Chocolate Pots mats (Figs. 7 and 8) appear to function in a similar manner, providing nucleating sites for accumulations of iron minerals and associated silica deposits. Iron and silica mineral deposition around bacterial cells including some cyanobacteria and *Chloroflexus* has been described for a variety of thermal environments [50–52].

The finer grained mineral casts of cyanobacteria that we observed below the mat surface with electron microscopy (Fig. 7) are consistent with the findings of Cady and Farmer [53] that the silicification process in thermal

←

Fig. 7. Transmission electron micrographs of thin sections of olive mat fixed in glutaraldehyde and OsO_4. (A) Longitudinal section through a narrow *Oscillatoria* filament showing lamellar membranes parallel to the long axis of the cell and mineral deposits in the extracellular matrix just exterior to a thick sheath (s). (B) Oblique and near cross-sections of the *Oscillatoria* filaments with each cell surrounded by mineral deposits external to the sheath. (C) Cross-section through a bundle of empty mineral casts and through several *Oscillatoria* filaments that are not heavily encased. This bundle is very similar in dimensions to streamers seen on some of the mats.

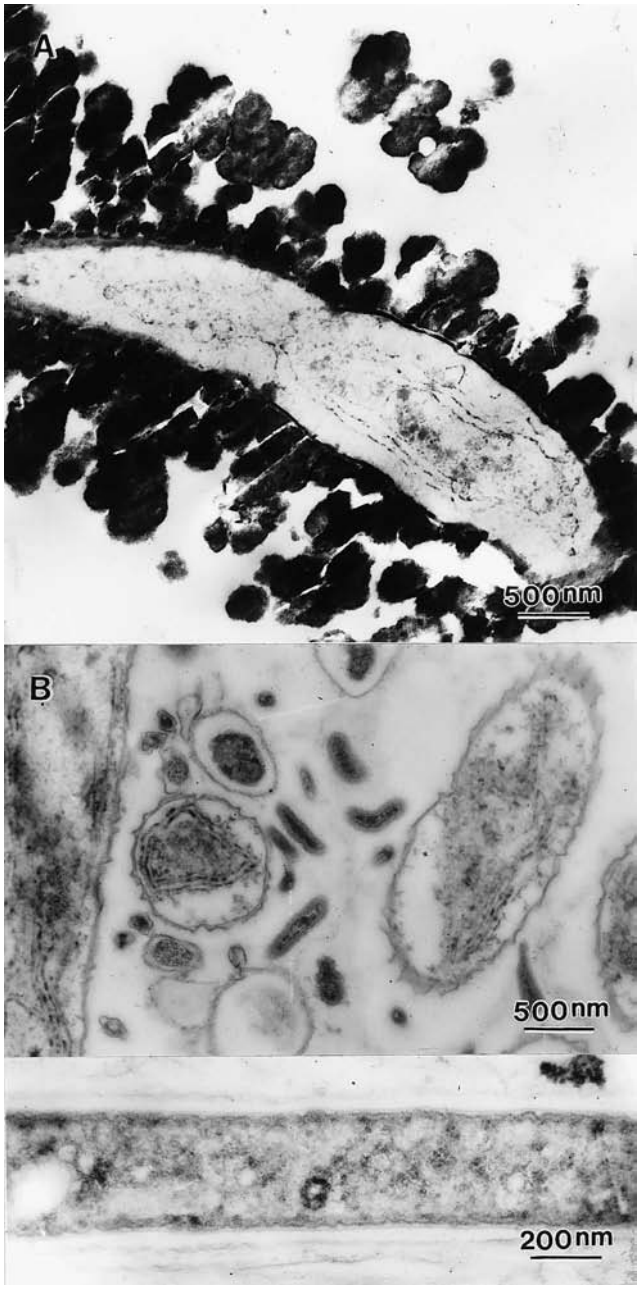

Fig. 8. Transmission electron micrographs of thin sections of *Synechococcus* mat fixed in OsO_4 and glutaraldehyde. (A) Mineral-encased degrading *Synechococcus* cell showing remains of concentric membranes. (B) Area of surface of mat showing much less mineral deposit, more potentially viable cells and greater diversity. *Synechococcus*, *Cyanothece* and a filament of *Chloroflexus* (bottom of figure) are seen as well as numerous unidentified small, curved rods with concentric membranes.

springs in the mid temperature ranges involves primarily mold formation around the cyanobacterial filaments. Wade et al. [25] also observed iron and silica mold formation in Chocolate Pots sediments but did not attribute the observed structures to any particular bacteria. Walter and Des Marais [54] suggest that this major silicification of microorganisms that occurs in hot springs over the temperature range of 30–59°C may lead to preservation of

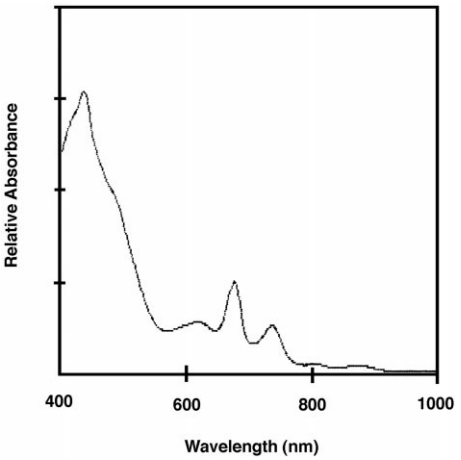

Fig. 9. Absorption spectrum (in vivo) of sonicated *Synechococcus*/*Chloroflexus* mat. Chl *a* peak at 677 nm. Bchl *c* at 737 nm and low Bchl *a* absorbance near 800 nm and 865 nm typical of *Chloroflexus* in hot spring mats. The spectrum also has large carotenoid absorbance (400–550 nm) and a maximum from phycocyanin near 620 nm.

structural orientations potentially useful in the search for remnants of past microbial life in hot springs on early Earth and Mars.

Some of the Chocolate Pots mats we studied were among the most rigid and cohesive for their thinness that we have observed in thermal springs (see Fig. 1M). We have presented microstructural evidence here that this cohesion and rigidity were facilitated by extensive mineral precipitation among the filamentous organisms. Early silicification seen as clear rigid gels may also be associated with iron accumulation (Fig. 1F,M–O).

3.8. Pigments

In vivo absorption spectra of all cyanobacterial mats (Figs. 9 and 10) revealed the presence of Chl *a* (677–679 nm) and phycobilins (620–625 nm). Peaks at 737 nm and

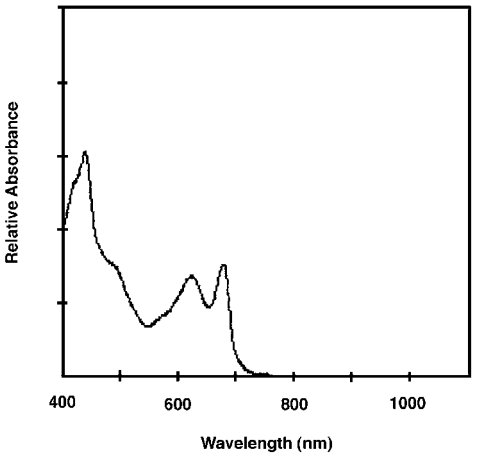

Fig. 10. Absorption spectrum of olive mat sonicated in buffer (in vivo). Carotenoids are present (400–500 nm) as well as Chl *a* (679 nm) and phycocyanin (625 nm).

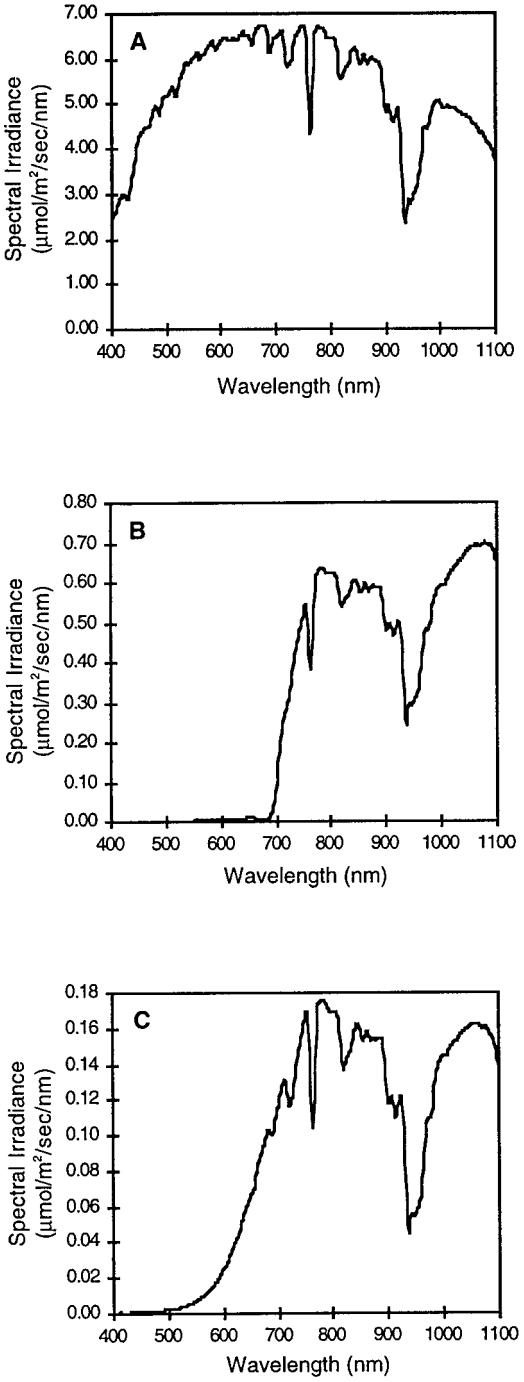

Fig. 11. Spectral irradiance in olive mats and plain iron sediments at Chocolate Pots Hot Springs measured by layering mats and sediments on top of the remote cosine receptor of a spectroradiometer. (A) Solar spectral irradiance measured at the surface of mat or sediment. (B) Spectral irradiance measured 0.5 mm beneath the surface layer of olive thin filaments. (C) Spectral irradiance measured beneath 0.5–1.0 mm of freshly settled iron oxides from a suspended hot spring iron deposit.

near 800 and 865 nm were consistent with the Bacteriochlorophyll (Bchl) *c* and *a*, respectively, from *Chloroflexus*, and were observed only in the *Synechococcus* mat (Fig. 9). Major absorption in the 400–500-nm range was due to carotenoids and Chl. Spectra of *Pseudanabaena* mats and *O. princeps* mats (data not shown) were similar to those of olive *Oscillatoria* mats (Fig. 10). The concentration of Chl *a* in the dense olive cyanobacterial mats calculated from methanol extracts ranged from 0.15–0.42 μg mm^{-3} in the top mm to 0.03–0.19 μg mm^{-3} in the second mm and were comparable to those reported for other cyanobacterial mats ([55]; Pierson, unpublished observations).

Methanol extracts of the iron sediments lacking conspicuous mats occasionally revealed the presence of Bchls along with Chl *a*. Chl *a* concentrations were much less in the sediments lacking obvious mats (0.01–0.02 μg mm^{-3} in the top mm and 0.001–0.008 μg mm^{-3} in the second mm).

Substantial NIR radiation which can be absorbed by Bchl *a* is available below the top mm of mats and sediments (Fig. 11) and penetrates down to a depth greater than 2 mm in some of the iron sediments [27]. Potentially damaging UV and near UV wavelengths are strongly attenuated by the iron sediments (Fig. 11) [10,20,27,56]. Consequently, within the top few mm of the sediments, there exists an ideal environment in which to seek a variety of anoxygenic photoferrotrophs such as those described by Ehrenreich and Widdel [7,8] with the capacity to oxidize Fe(II) in the presence of light without producing oxygen. In one sediment sample, we previously reported a light-dependent increase in pH without an increase in oxygen that could represent such a photometabolism [27]. An ephemeral in vivo peak detected near 970 nm (Fig. 12) in some mat/sediment samples could be indicative of a previously undescribed Bchl complex containing either Bchl *a* or *b*, or could be a transient NIR absorption maximum due to various oxidized iron minerals that also have absorption bands between 880 and 1000 nm [10].

3.9. A model for iron deposition by phototrophs

The data presented here suggest that the cyanobacterial

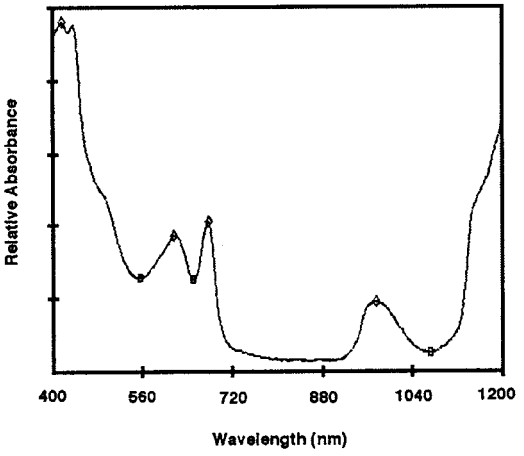

Fig. 12. Absorption spectrum of sediment containing narrow *Oscillatoria* filaments but not a well-developed olive mat sonically disrupted in buffer (in vivo). Carotenoids are present as well as Chl *a* (679 nm), phycocyanin (622 nm) and a peak at 970 nm that could be a Bchl peak or absorbance of a finely dispersed or soluble iron mineral complex.

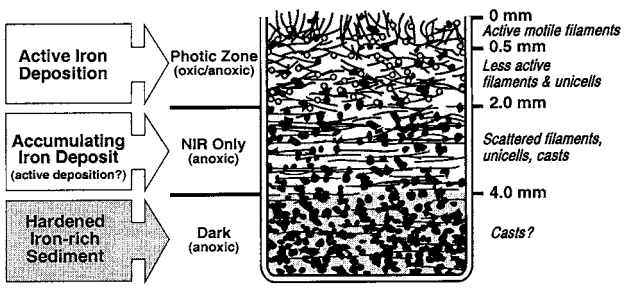

Fig. 13. Model for structural role of phototrophs in building an iron formation. Cyanobacteria form an active microbial mat which in these hot springs is a gelatinous deposit of microbes with iron and silica minerals. The left side of the figure recognizes three major zones of activity. The depth of the boundaries between zones (right side of figure) varies considerably among different mats. The photic zone exposed to visible light in the top 2 mm of the mat is the zone of active iron deposition (oxidation, mineral precipitation and entrapment). This zone undergoes diel fluctuations between oxic and anoxic conditions. Iron accumulates throughout this layer. Cyanobacteria are most active and vertically oriented in the top 0.5 mm of the mat. Deeper in the mat, only NIR radiation is available and conditions are progressively more anoxic. Compact iron accumulates with depth. See the text for further interpretation.

mats developing over the entire temperature range of the iron mounds are intimately involved in the stabilization and accumulation of this sinter. The CLSM images, motility observations and the electron micrographs indicate that some of the iron deposit is built from the accumulation of mineral precipitates intimately layered with degrading cyanobacterial cells and capped with a motile, photosynthetically active layer containing less iron around the individual cells. Fig. 13 illustrates a model for the development of such an iron deposit built from a photosynthetic microbial/mineral association. The initial flocculant iron oxides could become trapped by vertically oriented, motile filaments as in other freshwater mineralizing systems [57]. The sediments could then become consolidated and compacted deeper in the mat where some of the microbial remains would eventually degrade. The conspicuous layering of filamentous cells and amorphous orange/red oxidized iron particles was characteristic of all of the mats we studied (Fig. 1). The active motility of the olive filaments served to anchor new mat onto unconsolidated sediment as well as to bind precipitating sediment particles to the surface.

As in other microbial mats, actively motile photosynthetic filaments probably glide through the Chocolate Pots iron mats to position themselves optimally within an environment of steep and fluctuating gradients of light and oxygen. Since thickening accumulations of minerals and cells build up rapidly (we measured accretion rates of 0.05 mm per day in summer), gliding to the surface towards the light could be important for regaining photosynthetic activity and growth for filaments temporarily buried by iron precipitates. If some of the filaments are left behind, they may be able to survive for long periods of time (days or weeks) using alternative forms of metabolism such as fermentation of mat organic material or carbohydrate storage materials, as shown for *Oscillatoria terebriformis* in other hot spring mats [58]. We observed some remarkably healthy looking cyanobacteria deeper in the mats. Eventually, all the buried phototrophs would die and degrade. Many, however, apparently leave behind mineral casts or molds as evidence of their morphology (Fig. 7C) [25].

3.10. Impact of cyanobacterial photosynthetic activity on the iron depositional microenvironment and relevance to BIFs

Analysis of the cyanobacterial mats on the iron mounds with microelectrodes [27] has shown that the cyanobacterial photosynthetic activity substantially alters the sediment environment, creating conditions that could enhance the rate of iron oxidation. In the light, cyanobacterial mats produce oxygen concentrations in excess of air saturation values and raise the pH above 8.0 [27]. In the dark, oxygen levels decrease, falling to zero usually within the top 2 mm [27]. Increased oxygen and pH in the light could contribute to higher than ambient rates of iron oxidation.

Agresti et al. [24] and Wade et al. [25] postulated that the increase in pH required for carbonate precipitation in the formation of siderite could be attributed to sulfate reduction. However, despite the presence of sulfate in the source waters (Table 1), we have not yet found evidence for sulfide production in the top 4.0 mm of these mats even in the dark. Agresti et al. [24] and Wade et al. [25] did not report iron sulfide minerals in their analyses. It is certainly possible that rapid sulfur cycling is occurring in these mats. We demonstrated, however, that large light-dependent increases in pH occurred over a broad depth range in many microbial sediments at Chocolate Pots due to photosynthetic activity of the cyanobacteria and perhaps anoxygenic phototrophs [27]. We thus suggest that photosynthesis could be influencing the formation of siderite. Iron-reducing bacteria below the oxic zone could also raise the pH encouraging siderite formation [59].

To our knowledge, such a massive and intimate association of photosynthetic cyanobacteria and *Chloroflexus* sp. with a growing iron deposit, including the presence of abundant iron-encased single cells and filaments, has not previously been reported. Iron springs, seeps and other iron deposits are usually associated with chemolithoautotrophic bacteria [1,5,31,60]. Low pH is inhibitory to cyanobacteria. Acidic iron environments are thus dominated by chemoautotrophs or eukaryotic algae when phototrophs are present (unpublished observations). Cyanobacteria may also be inhibited near neutral pH by the higher iron or other metal concentrations in many other springs.

Chemotrophic bacteria probably have an active role in the accumulation of iron in some environments. In acidic environments, iron oxidation without microbial metabolic facilitation is slow [61]. Iron oxidation rates can also be

slow in the absence of microbial facilitation in neutral environments due to relatively low oxygen levels [31,60]. At Chocolate Pots, cyanobacterial photosynthetic activity may enhance iron oxidation rates and alter iron mineral deposition by increasing pH and oxygen concentration [27]. As described here, cyanobacterial walls and sheaths provide mineral nucleating sites and the motility of filaments aids in trapping precipitates thus retaining and stabilizing the mineral deposit. The abundance and activity of the phototrophs create discrete and fluctuating ecological microzones that are likely to contain diverse chemotrophic iron bacteria that could contribute to a vigorous cycling of iron.

Klein and Beukes [62] define iron formations as 'a chemical sediment, typically thin-bedded or laminated, whose principal chemical characteristic is an anomalously high content of iron, commonly but not necessarily containing layers of chert'. The authors point out that the mineralogy of iron formations varies widely including oxides, carbonates, sulfides and silicates, and is largely determined by diagenetic and metamorphic processes. While the actual weight percent of iron in the rock is defined over a narrow range (23–34), the ratio of ferric iron to total iron varies considerably from 0.05 to 0.58 with a mean of 0.42 and one anomalously high value of 0.97 (the Rapitan Formation) [62]. Chocolate Pots Hot Springs is depositing an iron formation containing oxides, carbonates and silicates [24,25,38]. Our microstructural observations reported here of the active zone of deposition reveal microbial/mineral assemblages strikingly similar to images reported by Cloud and Licari [63] which were attributed to cyanobacteria. Similar mineral-encased bacteria in a thermal environment were observed by Konhauser and Ferris [51] who noted their potential relevance to iron formations. Determining the biogenicity of such ancient structures [63] can be fraught with difficulty, however [64]. While the iron formation at Chocolate Pots Hot Springs is not analogous to Precambrian BIFs formed in deep basins [65], it does provide a test case in which to analyze the role of and potential mineralogical and isotopic signals produced by the active photosynthetic primary producers (cyanobacteria and other photosynthetic prokaryotes) intimately associated with a high iron depositional environment.

Acknowledgements

This work was supported by Grant NAGW-5090 from the NASA Exobiology Program to B.K.P. During 1997, B.K.P. was supported by a John Lantz Senior Research Fellowship from the University of Puget Sound to conduct research at Cornell University. Research funds were also provided by the University of Puget Sound Enrichment Committee to B.K.P. and M.N.P. We thank the National Park Service for permission to conduct research in Yellowstone National Park. We also thank W.C. Ghiorse for instruction in and permission to use the CLSM in the Department of Microbiology at Cornell University. We thank Larry Anthony, Scott Sheffield, Mark Kasprowicz and Scott Pierson for computer graphics assistance and R.W. Castenholz, University of Oregon, for help in identifying cyanobacteria. Water analysis (Table 1) was done by Water Management Laboratories, Tacoma, WA, USA.

References

[1] Ehrlich, H.L. (1996) Geomicrobiology, 3rd edn. Marcel Dekker, NY.
[2] Ghiorse, W.C. and Ehrlich, H.L. (1992) Microbial biomineralization of iron and manganese. In: Biomineralization Processes of Iron and Manganese: Modern and Ancient Environments (Skinner, H.C.W. and Fitzpatrick, R.W., Eds.), pp. 75–99. Catena Verlag, Cremlingen-Destedt.
[3] Lovley, D.R. (1992) Microbial oxidation of organic matter coupled to the reduction of Fe(III) and Mn(IV) oxides. In: Biomineralization Processes of Iron and Manganese: Modern and Ancient Environments (Skinner, H.C.W. and Fitzpatrick, R.W., Eds.), pp. 101–114. Catena Verlag, Cremlingen-Destedt.
[4] Nealson, K.H. and Little, B. (1997) Breathing manganese and iron: solid-state respiration. Adv. Appl. Microbiol. 45, 213–239.
[5] Emerson, D. and Moyer, C. (1997) Isolation and characterization of novel iron-oxidizing bacteria that grow at circumneutral pH. Appl. Environ. Microbiol. 63, 4784–4792.
[6] Straub, K.L., Benz, M., Schink, B. and Widdel, F. (1996) Anaerobic, nitrate-dependent microbial oxidation of ferrous iron. Appl. Environ. Microbiol. 62, 1458–1460.
[7] Ehrenreich, A. and Widdel, F. (1994) Anaerobic oxidation of ferrous iron by purple bacteria, a new type of phototrophic metabolism. Appl. Environ. Microbiol. 60, 4517–4526.
[8] Ehrenreich, A. and Widdel, F. (1994) Phototrophic oxidation of ferrous minerals - a new aspect in the redox microbiology of iron. In: Microbial Mats, Vol. G35 (Stal, A.J. and Caumette, P., Eds.), pp. 393–402. NATO ASI Series, Springer-Verlag, Berlin.
[9] Widdel, F., Schnell, S., Heising, S., Ehrenreich, A., Assmus, B. and Schink, B. (1993) Ferrous iron oxidation by anoxygenic phototrophic bacteria. Nature 362, 834–836.
[10] Cornell, R.M. and Schwertmann, U. (1996) The Iron Oxides: Structure, Properties, Reactions, Occurrence and Uses. VCH Verlagsgesellschaft, Weinheim.
[11] Wächtershäuser, G. (1988) Before enzymes and templates: theory of surface metabolism. Microbiol. Rev. 52, 452–484.
[12] Hartman, H. (1992) Conjectures and reveries. Photosynth. Res. 33, 171–176.
[13] Mauzerall, D. (1992) Light, iron, Sam Granick and the origin of life. Photosynth. Res. 33, 163–170.
[14] Cloud, P. (1973) Paleoecological significance of the banded iron-formation. Econ. Geol. 68, 1135–1143.
[15] Schopf, J.W. (1993) Microfossils of the early Archean Apex chert: new evidence of the antiquity of life. Science 260, 640–646.
[16] Cohen, Y. (1984) Comparative N and S cycles. In: Current Perspectives in Microbial Ecology (Klug, M.J. and Reddy, C.A., Eds.), pp. 435–441. American Society for Microbiology, Washington, DC.
[17] Cohen, Y. (1989) Photosynthesis in cyanobacterial mats and its relation to the sulfur cycle: a model for microbial sulfur interactions. In: Microbial Mats: Physiological Ecology of Benthic Microbial Communities (Cohen, Y. and Rosenberg, E., Eds.), pp. 22–36. American Society for Microbiology, Washington, DC.
[18] Hartman, H. (1984) The evolution of photosynthesis and microbial mats: a speculation on the banded iron formations. In: Microbial

Mats: Stromatolites (Cohen, Y., Castenholz, R.W. and Halvorson, H.O., Eds.), pp. 449–453. Alan R. Liss, New York.
[19] Olson, J.M. and Pierson, B.K. (1987) Evolution of reaction centers in photosynthetic prokaryotes. Int. Rev. Cytol. 108, 209–248.
[20] Pierson, B.K. (1994) The emergence, diversification, and role of photosynthetic eubacteria. In: Early Life on Earth, Nobel Symposium No. 84 (Bengtson, S., Ed.), pp. 161–180. Columbia University Press, New York.
[21] Pierson, B.K. and Olson, J.M. (1989) Evolution of photosynthesis in anoxygenic photosynthetic procaryotes. In: Microbial Mats: Physiological Ecology of Benthic Microbial Communities (Cohen, Y. and Rosenberg, E., Eds.), pp. 402–427. American Society for Microbiology, Washington, DC.
[22] Kump, L. (1993) Bacteria forge a new link. Nature 362, 790–791.
[23] Heising, S., Richter, L., Ludwig, W. and Schink, B. (1999) *Chlorobium ferrooxidans* sp. nov., a phototrophic green sulfur bacterium that oxidizes ferrous iron in coculture with a '*Geospirillum*' sp. strain. Arch. Microbiol. 172, 116–124.
[24] Agresti, D.G., Wdowiak, T.J., Wade, M.L., Armendarez, L.P. and Farmer, J.D. (1997) Mössbauer spectroscopy of thermal springs iron deposits as Martian analogs. In: Conference On Early Mars: Geologic and Hydrologic Evolution, Physical and Chemical Environments, and the Implications For Life (Clifford, S.M., Treiman, A.H., Newson, H.E. and Farmer, J.D., Eds), pp. 1–2. Lunar and Planetary Institute Contribution No. 916.
[25] Wade, M.L., Agresti, D.G., Wdowiak, T.J., Armendarez, L.P. and Farmer, J.D. (1999) A Mössbauer investigation of iron-rich terrestrial hydrothermal vent systems: lessons for Mars exploration. J. Geophys. Res. 104, 8489–8507.
[26] Wilson, C.L., Hinman, N.W. and Brown, C.F. (1998) Diel cycling of hydrogen peroxide in surface geothermal waters: possible formation from metal redox reactions, abstr. 1406. In: Lunar and Planetary Science Conference XXIX. Lunar and Planetary Inst., Houston, TX.
[27] Pierson, B.K., Parenteau, M.N. and Griffin, B.M. (1999) Phototrophs in high-iron-concentration microbial mats: Physiological ecology of phototrophs in an iron-depositing hot spring. Appl. Environ. Microbiol. 65, 5474–5483.
[28] Parenteau, M.N., Griffin, B.M. and Pierson, B.K. (1996) Phototrophs in high iron environments, abstr. N-36. In: Abstracts of the 96th General Meeting of the American Society for Microbiology. Am. Soc. for Microbiol., Washington, DC.
[29] Pierson, B.K. and Parenteau, M.N. (1999) Structural analysis of phototrophic bacteria and minerals in high iron microbial mats, abstr. N-12. In: Abstracts of the 99th General Meeting of the American Society for Microbiology. Am. Soc. for Microbiol., Washington, DC.
[30] Greenberg, A.E., Clesceri, L.S. and Eaton, A.D. (1992) Standard Methods for the Examination of Water and Wastewater, 18th edn. Am. Public Health Assoc., Washington, DC.
[31] Emerson, D. and Revsbech, N.P. (1994) Investigation of an iron-oxidizing microbial mat community located near Aarhus, Denmark: field studies. Appl. Environ. Microbiol. 60, 4022–4031.
[32] Stookey, L.L. (1970) Ferrozine - a new spectrophotometric reagent for iron. Anal. Chem. 42, 779–781.
[33] Castenholz, R.W. (1976) The effect of sulfide on the bluegreen algae of hot springs. I. New Zealand and Iceland. J. Phycol. 12, 54–68.
[34] Ghiorse, W.C., Miller, D.N., Sandoli, R.L. and Siering, P.L. (1996) Applications of laser scanning microscopy for analysis of aquatic microhabitats. Microsc. Res. Tech. 33, 73–86.
[35] Pierson, B.K., Valdez, D., Larsen, M., Morgan, E. and Mack, E.E. (1994) *Chloroflexus*-like organisms from marine and hypersaline environments: distribution and diversity. Photosynth. Res. 41, 35–52.
[36] Pierson, B.K., Oesterle, A. and Murphy, G.L. (1987) Pigments, light penetration and photosynthetic activity in the multilayered microbial mats of Great Sippewissett Salt Marsh, Massachusetts. FEMS Microbiol. Ecol. 45, 365–376.
[37] Pierson, B.K., Sands, V.M. and Frederick, J.L. (1990) Spectral irradiance and distribution of pigments in a highly layered marine microbial mat. Appl. Environ. Microbiol. 56, 2327–2340.
[38] Allen, E.T. and Day, A.L. (1935) Hot Springs of the Yellowstone National Park. Carnegie Institute of Washington, Publication #466, Waverly Press, Baltimore, MD.
[39] Whittlesey, L. (1988) Wonderland Nomenclature: a History of the Place Names of Yellowstone National Park, pp. 277–278. Montana Historical Press, Prepared by the Geyser Observation and Study Association, Sacramento, CA.
[40] Rowe, J.J., Fournier, R.O. and Morey, G.W. (1973) Chemical Analysis of Thermal Waters in Yellowstone National Park, Wyoming, 1960–65. Geological Survey Bulletin 1303.
[41] Stauffer, R.E., Jenne, E.A. and Ball, J.W. (1980) Chemical Studies of Selected Trace Elements in Hot-Spring Drainages of Yellowstone National Park. Geohydrology of Geothermal Systems. Geological Survey Professional Paper 1044-F.
[42] Little, B.J., Wagner, P.A. and Lewandowski, Z. (1997) Spatial relationships between bacteria and mineral surfaces. In: Geomicrobiology: Interactions Between Microbes and Minerals, v. 35 (Banfield, J.F. and Nealson, K.H., Eds.), pp. 123–159. Reviews in Mineralogy, Mineralogical Society of America, Washington, DC.
[43] Castenholz, R.W. (1984) Composition of hot spring microbial mats: a summary. In: Microbial Mats: Stromatolites (Cohen, Y., Castenholz, R.W. and Halvorson, H.O., Eds.), pp. 101–119. Alan R. Liss, New York.
[44] Hanada, S., Hiraishi, A., Shimada, K. and Matsuura, K. (1995) Isolation of *Chloroflexus aurantiacus* and related thermophilic phototrophic bacteria from Japanese hot springs using an improved isolation procedure. J. Gen. Appl. Microbiol. 41, 119–130.
[45] Castenholz, R.W. and Pierson, B.K. (1995) Ecology of thermophilic anoxygenic phototrophs. In: Anoxygenic Photosynthetic Bacteria (Blankenship, R.E., Madigan, M.T. and Bauer, C.E., Eds.), pp. 87–103. Kluwer Academic Publ., Dordrecht.
[46] Fortin, D., Ferris, F.G. and Beveridge, T.J. (1997) Surface-mediated mineral development by bacteria. In: Geomicrobiology: Interactions Between Microbes and Minerals, v. 35 (Banfield, J.F. and Nealson, K.H., Eds.), pp. 161–180. Reviews in Mineralogy, Mineralogical Society of America, Washington, DC.
[47] Douglas, S. and Beveridge, T.J. (1998) Mineral formation by bacteria in natural microbial communities. FEMS Microbiol. Ecol. 26, 79–88.
[48] Konhauser, K.O. (1997) Bacterial iron biomineralisation in nature. FEMS Microbiol. Rev. 20, 315–326.
[49] Pentecost, A., Bayari, S. and Yesertener, C. (1997) Phototrophic microorganisms of the Pamukkale Travertine, Turkey: their distribution and influence on travertine deposition. Geomicrobiol. J. 14, 269–283.
[50] Ferris, F.G., Beveridge, T.J. and Fyfe, W.S. (1986) Iron-silica crystallite nucleation by bacteria in a geothermal sediment. Nature 320, 609–611.
[51] Konhauser, K.O. and Ferris, F.G. (1996) Diversity of iron and silica precipitation by microbial mats in hydrothermal waters, Iceland: implications for Precambrian iron formations. Geology 24, 323–326.
[52] Schultze-Lam, S., Ferris, F.G., Konhauser, K.O. and Wiese, R.G. (1995) In situ silicification of an Icelandic hot spring microbial mat: implications for microfossil formation. Can. J. Earth Sci. 32, 2021–2026.
[53] Cady, S.L. and Farmer, J.D. (1996) Fossilization processes in siliceous thermal springs: trends in preservation along thermal gradients. In: Evolution of Hydrothermal Ecosystems on Earth (and Mars?), pp. 150–173. Ciba Foundation Symposium 202, John Wiley and Sons.
[54] Walter, M.R. and Des Marais, D.J. (1993) Preservation of biological information in thermal spring deposits: developing a strategy for the search for fossil life on Mars. ICARUS 101, 129–143.
[55] van Gemerden, H., Tughan, C.S., de Wit, R. and Herbert, R.A. (1989) Laminated microbial ecosystems on sheltered beaches in Scapa Flow, Orkney Islands. FEMS Microbiol. Ecol. 62, 87–102.

[56] Pierson, B.K., Mitchell, H.K. and Ruff-Roberts, A.L. (1993) *Chloroflexus aurantiacus* and ultraviolet radiation: implications for Archean shallow-water stromatolites. Orig. Life Evol. Biosph. 23, 243–260.
[57] Freytet, P. and Verrecchia, E.P. (1998) Freshwater organisms that build stromatolites: a synopsis of biocrystallization by prokaryotic and eukaryotic algae. Sedimentology 45, 535–563.
[58] Richardson, L.L. and Castenholz, R.W. (1987) Enhanced survival of the cyanobacterium *Oscillatoria terebriformis* in darkness under anaerobic conditions. Appl. Environ. Microbiol. 53, 2151–2158.
[59] Coleman, M.L., Hedrick, D.B., Lovley, D.R., White, D.C. and Pye, K. (1993) Reduction of Fe(III) in sediments by sulphate-reducing bacteria. Nature 361, 436–438.
[60] Holm, N.G. (1987) Biogenic influences on the geochemistry of certain ferruginous sediments of hydrothermal origin. Chem. Geol. 63, 45–57.
[61] Singer, D.C. and Stumm, W. (1970) Acidic mine drainage: the rate-determining step. Science 167, 1121–1123.
[62] Klein, C. and Beukes, N.J. (1992) Time distribution, stratigraphy, and sedimentologic setting, and geochemistry of precambrian iron-formations. In: The Proterozoic Biosphere: A Multidisciplinary Study (Schopf, J.W. and Klein, C., Eds.), pp. 139–146. Cambridge University Press.
[63] Cloud, P.E. and Licari, G.R. (1968) Microbiotas of the banded iron formations. Proc. Natl. Acad. Sci. USA 61, 779–786.
[64] Walter, M.R. and Hofmann, H.J. (1983) The palaeontology and palaeoecology of Precambrian iron-formations. In: Iron-Formation: Facts and Problems (Trendall, A.F. and Morris, R.C., Eds.), pp. 373–400. Elsevier Science Publishers B.V., Amsterdam.
[65] Beukes, N.J. and Klein, C. (1992) Models for iron-formation deposition. In: The Proterozoic Biosphere: a Multidisciplinary Study (Schopf, J.W. and Klein, C., Eds.), pp. 147–151. Cambridge University Press.